Low-Noise 6-8 GHz Receiver

Jagadheep D. Pandian, Lynn Baker, German Cortes, Paul F. Goldsmith, Avinash A. Deshpande, Rajagopalan Ganesan, Jon Hagen, Lisa Locke, Niklas Wadefalk, and Sander Weinreb

The science of radio astronomy involves the detection of radio waves from astronomical objects in space. Astronomical objects emit radio waves by a variety of processes, including thermal radiation from gas and dust in the interstellar medium, synchrotron emission from relativistic electrons spiraling around magnetic fields, free-free emission from electrons in ionized regions, and spectral line radiation from atomic and molecular transitions. Since the sources that radio astronomers observe are generally very distant, the intensity of radio waves from them is extremely low. This is compounded by the fact that the bandwidth of spectral lines is very small. For example, a cloud of atomic hydrogen with internal motions of 5 km/s emits only over a bandwidth of 25 kHz. A source at temperature T produces a maximum signal power $P = kTB$, where k is the Boltzmann's constant (1.38×10^{-23} W/K-Hz) and B is

Jagadheep D. Pandian (jagadheep@astro.cornell.edu) is with Cornell University. Lynn Baker and German Cortes are with NAIC/Cornell University. Paul F. Goldsmith is with Cornell University/Jet Propulsion Laboratory. Avinash A. Deshpande is with Arecibo Observatory/Raman Research Institute. Rajagopalan Ganesan and Jon Hagen are with Arecibo Observatory. Lisa Locke is with Arecibo Observatory/NRAO, Socorro. Niklas Wadefalk is with Jet Propulsion Laboratory/Chalmers Institute of Technology. Sander Weinreb is with Jet Propulsion Laboratory.

 1527-3342/06/$20.00©2006 IEEE

the bandwidth. For a relatively warm interstellar cloud at 100 K, the signal power is no greater than 3.5×10^{-17} W, a very weak signal. Some signals are nonthermal and can be stronger than this, but astronomers typically make maps of the radio sky, which requires pointing the antenna successively in different directions. To cover a significant area of the sky with a small antenna beam width, thousands to many millions of separate pointings and integrations are needed. As a result, the time that can be spent analyzing the signal from any one direction is limited. A very sensitive system to detect and analyze radio astronomical signals is thus extremely desirable.

All radio telescope systems have three basic components: an antenna to collect the incident radiation, a receiver to detect this radiation, and a back-end system, which analyzes the signals. The functioning of the back-end system depends on what type of signal is being observed—it may simply measure the total power in a broadband or continuum signal, or it may split the signal into several relatively narrow bands and measure the power in each, thereby producing a spectrum of the incident radiation. The most familiar type of radio telescope comprises a parabolic dish that focuses radiation into the receiver with or without the aid of a secondary reflector. Dual reflector radio antenna systems can be of the Cassegrain or Gregorian type, similar to their counterparts at optical wavelengths. The overall sensitivity of the system is controlled primarily by the size and the efficiency of the antenna and the sensitivity of the receiver.

The 305 m Arecibo telescope, which is part of the National Astronomy and Ionosphere Center and operated by Cornell University under a cooperative agreement with the National Science Foundation, is the largest single dish radio telescope in the world (Figure 1). The projected area of the complete surface is just over 73,000 m^2, which is more than that of 17 football fields. Unlike most radio telescopes, the primary reflector at Arecibo is spherical rather than parabolic. Since a sphere focuses radiation into a line rather than a point, line feeds were used to detect the radiation from its initial operation in the early 1960s until the late 1990s. The Gregorian system was commissioned in 1997; the Gregorian dome and the line feed, still used for 430 MHz, move in elevation on the feed arm, the lower part of which is a curved track moving near the paraxial surface. The feed arm also rotates in azimuth. The moving parts are held by a triangular structure, which is itself suspended on steel cables running from three towers surrounding the primary reflector. The inward force of these cables on the towers is balanced by backstay cables extending radially from each of the towers.

A line feed is a very specialized traveling wave antenna, which combines the radiation collected by various portions of the spherical primary reflector with the proper phase delays, thus correcting the substantial spherical aberration of the reflector (Figure 2). The line feed system collects radiation focused by the spherical primary, while the Gregorian system uses two additional reflectors to focus radiation to a point where the feed horn of the receiver is located. The value of the phase correcting characteristic of a line feed is offset in part by their very narrow bandwidths (<50 MHz) and lack of any tunability. Over the course of three decades, only a handful of line feeds were constructed, covering narrow portions of the frequency range extending to 2.4 GHz.

The Arecibo telescope had a major upgrade in the mid 1990s [1]. The major part of this project consisted of installing a pair of aspheric reflectors near the paraxial surface, where radiation from the primary is most tightly focused. These two reflectors were designed to compensate for the phase errors in the spherical primary reflector, but since they are reflective, the phase correction is essentially independent of frequency. Thus, with the so-called Gregorian system, the Arecibo telescope focuses radiation essentially perfectly at frequencies as high as 10 GHz and with bandwidths up to several gigahertz. This has resulted in a dramatic

Figure 1. *Aerial view of the Arecibo radio telescope after the Gregorian system was commissioned in 1997.*

Figure 2. *A schematic showing the optics for the line feed and Gregorian systems at the Arecibo radio telescope.*

increase in the range of astronomical observations that can be carried out and also has significantly improved the system's sensitivity due to better illumination of the primary reflector. As shown in Figure 2, the two Gregorian reflectors are enclosed by a protective dome. The radio signals enter through the circular aperture at the bottom left of the dome and follow the paths indicated by the red lines, reflecting from the secondary then the tertiary. With the Gregorian system, the Arecibo telescope focuses radiation to a point (as indicated in the figure) or more accurately, to a spot where it is collected by a fairly typical feed horn, which in this case is oriented downward.

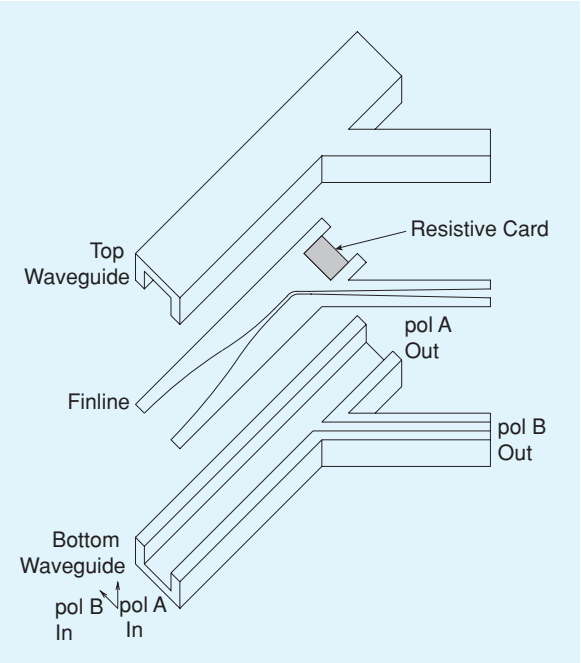

Figure 3. *A schematic of the finline OMT used to separate incoming fields into two orthogonal polarization components.*

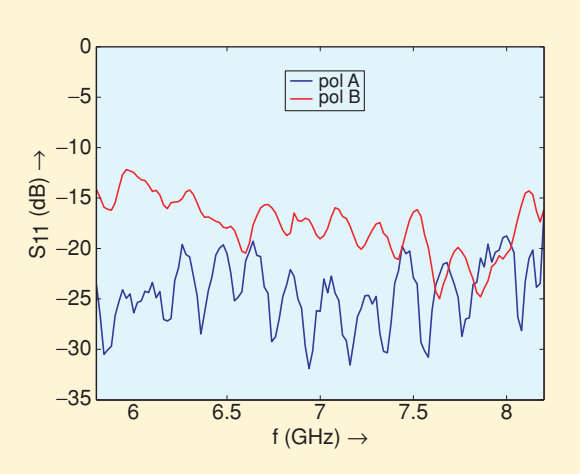

Figure 4. *Measured return loss of the OMT. The blue curve is for polarization A, which passes straight through; the red curve is for polarization B, which passes through the finline.*

Thus, for the Arecibo Gregorian receivers, as for almost all radio astronomical systems, the first component is the feed horn. The feed horn converts the incident free space transverse electromagnetic radiation into a waveguide transverse electric or transverse magnetic mode. In this sense, the angular width of the receiving power pattern of the feedhorn must match the angular size of the cone of radiation coming from the antenna. Taking advantage of the reciprocity principle, we can also think of replacing the receiver by a transmitter, and thus the feedhorn radiates a signal with an angular transmitting power pattern, which is the same as the receiving power pattern. This pattern of the feed horn determines the efficiency with which the antenna operates, in particular, the aperture efficiency and antenna gain (relevant for point sources) and the main beam efficiency (relevant for extended sources). The feed horn also needs to have a very low reflection coefficient so that most of the signal is transmitted to the receiver. The output waveguide from the feed horn typically propagates both polarizations of the incoming signal.

Since most signals from space are unpolarized or, if partially polarized, have a random polarization angle, a simple conversion of the electromagnetic signal from space into a guided wave in a single mode waveguide will result in the loss of approximately half the signal. To attain full efficiency as well as to measure the polarization state of the incident signal, it is necessary to have a device that separates the two orthogonal polarizations before they are each channeled into a single mode waveguide. This task is accomplished by the ortho-mode transducer (OMT). The OMT needs to have a return loss of 15 dB or better over the entire band of interest, in addition to having a low insertion loss. To carry out good polarimetry, the cross polarization introduced by the OMT should be less than that induced by the feed horn. The OMT is typically the most challenging part of a dual polarization broadband receiver design.

The outputs from the OMT are amplified using low-noise amplifiers. The low-noise amplifier and the stage following it are the primary contributors to the receiver noise temperature, since noise from successive components of the receiver are suppressed by the gain of the amplifier. To achieve very low noise, the amplifier and the OMT are typically cooled to temperatures that can be as low as 2–15 K. This requires the receiver components to be placed in an evacuated dewar. Moreover, since most designs keep the feed horn at room temperature (due to its relatively large size), there needs to be a device that thermally isolates the feed horn from the OMT while maintaining continuity for the RF signal. This device is called a thermal break and typically uses choke grooves to minimize signal reflections.

The upgrade of the Arecibo telescope allowed operations up to a frequency of 10 GHz. Before 2004, the telescope had receivers for all frequencies between 1.1 and 10 GHz, except for the 6–8 GHz frequency range of C-

Band (4–8 GHz). The band includes the 6.668 GHz spectral line of methanol, which emits stimulated radiation with very high brightness temperature ($> 10^{10}$ K) under conditions found around sites of massive star formation. Hitherto, all 6.7 GHz methanol maser studies have been carried out using Australian and European telescopes.

This article reports on the 6–8 GHz receiver that was installed on the telescope in early 2004. With the installation of this instrument, Arecibo has continuous frequency coverage between 1.1 and 10 GHz. The following discusses the receiver design and presents the measured performance in detail.

The Ortho-Mode Transducer

We adopted a finline design for the OMT from the work of Chattopadhyay and Carlstrom [2] (Figure 3). A finline OMT consists of a thin metallic fin that is set inside a square or circular waveguide. The polarization mode which has an electric field parallel to the fin, is converted from a waveguide mode into a finline mode whose energy is confined to the space between the fin. This energy can then be brought out by curving the fin and bringing it out of the wall of the waveguide, after which it is converted back into a waveguide mode by a gradual outward taper. The orthogonal polarization has electric field perpendicular to the fin and passes unperturbed if the fin is sufficiently thin. A resistive card suppresses any unwanted modes at the termination of the fin.

The design of Chattopadhyay and Carlstrom involved the removal of the finline mode through a 45° bend, which was found to give better cross polarization and isolation performance compared to a 90° bend. We took their prototype design for X-Band and scaled it to our band with some modifications. We replaced the multiple transitions between the finline and the normal waveguide after the bend with a single, longer transition, as a traveling wave device is likely to give a better performance with a longer transition. Using the same reasoning, we also lengthened the initial transition in the finline from square waveguide to the narrow gap.

The rectangular waveguide used for 6–8 GHz is WR137, which has dimensions of 3.48×1.58 cm (1.372×0.622 in). Hence, the square waveguide input for the OMT has an interior dimension of 3.48 cm (1.372 in). This is tapered to 0.038 cm (0.015 in) in the finline through two circular arcs over a length of 27.13 cm (10.68 in). Following the 45° bend, the narrow gap is expanded to the standard dimension of 1.58 cm (0.622 in) over a length of 20.32 cm (8.0 in). The fin is made out of a 0.13 cm (0.05 in) thick aluminum sheet.

Figures 4–7 show the measured performance (at room temperature) of the OMT fabricated from the design above. The measurements were taken with one port being terminated by a tapered ferrite rod and the other two ports being connected to the network analyzer. The return loss conformed to our design goal save for a small portion in the band edge near 6 GHz.

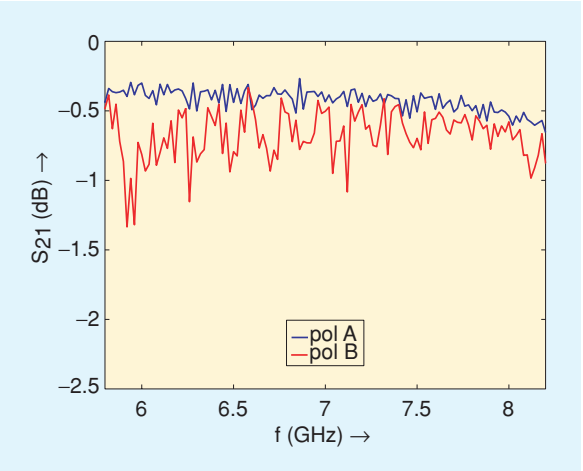

Figure 5. *Measured insertion loss of the OMT. The blue curve is for polarization A, which passes straight through; the red curve is for polarization B, which passes through the finline.*

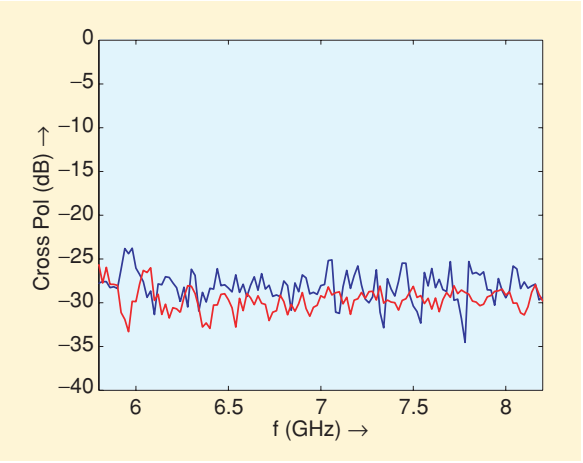

Figure 6. *Measured cross-polarization isolation of the OMT. The blue line is for input polarization A when the output is measured at pol B, and the red curve is for polarization B input polarization when the output is measured at pol A. The third port is terminated appropriately during these measurements.*

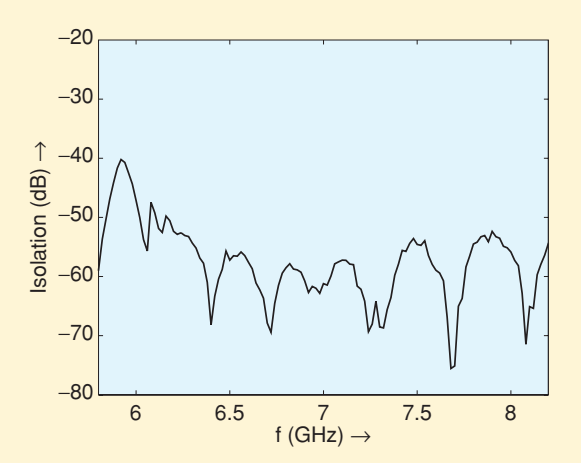

Figure 7. *Measured isolation between the two output ports of the OMT.*

TABLE 1. Calculated Overall Antenna Parameters At The Input Flange of the Arecibo Radio Telescope's Feed Horn.

Frequency GHz	$\eta_{Aperture}$ %	η_{Illum} %	η_{Beam} %	X-Pol dB	T_A K
6.0	82.2	93.6	80.2	−28.0	14.2
7.0	81.7	93.6	81.3	−29.0	13.0
8.0	78.5	90.1	81.8	−26.0	11.8

$\eta_{Aperture}$ is the effective collecting area of the telescope divided by the illuminated area 3.98×10^4 m^2); η_{Illum} is the reduction in efficiency due to nonuniform illumination of the antenna; η_{Beam} is the fraction of total radiated power within −10 dB level of peak of power pattern; X-pol is the cross-polarization level in the antenna far field; T_A is the antenna temperature referred to the feed horn flange, and includes contributions from the cosmic microwave background (2.73 K), emission from the atmosphere, and also radiation from the dome and spillover radiation from the ground. Note that efficiency reduction due to surface errors is not included.

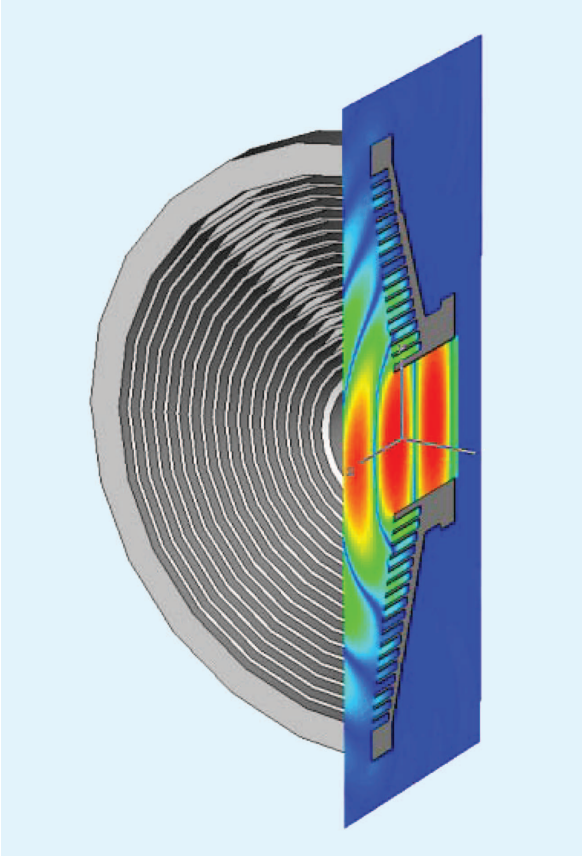

Figure 8. *Calculated E_{VERT} projected on a cross section of the corrugated horn at 7 GHz.*

The isolation (coupling between the two output ports when the input is terminated) was 50 dB or better over the entire band, and the cross polarization isolation was better than 25 dB throughout. The insertion loss is primarily ohmic, and its contribution to the noise temperature would drop significantly when the device is cooled from room temperature to around 15 K.

The Feed Horn

The 6–8 GHz feed horn used in the receiver is a wide flare angle corrugated horn [3]. For the present design, we chose a 78° flare angle that provides an edge taper level of −15 dB at the edge of the tertiary Gregorian reflector (approximately 60° off axis) in the middle of the frequency band. In addition, we decided to have the corrugations running parallel to the horn axis for fabrication purposes.

The designed horn has an aperture diameter of 21.6 cm (8.5 in) and a circular waveguide input diameter of 4.95 cm (1.95 in). The horn design was verified using Ansoft HFSS and CST Microwave Studio. Figure 8 shows the calculated E_{VERT} field projected on a cross section of the corrugated horn at 7 GHz; notice the profile of the corrugations. The calculated input reflection coefficient (Figure 9) is better than 26 dB across the band.

We fabricated two horns (I and II) since the receiver will be upgraded to a dual beam receiver sometime in the near future. Only horn I has been installed in the receiver to date. We measured the radiation patterns of both horns with cuts at the E and H planes and at 45° for θ between −90° and +90°, with linear polarization excitation. A comparison of the measured data of horn I with the calculated field patterns is presented in Figures 10–12. In each, we show two copolar pattern cuts at 0° and 90° and a cross-polar pattern cut at 45°. We find a good correlation between calculated (continuous lines) and measured data (dots). The measured cross polarization levels are below −24 dB except at 8 GHz, where they are −20 dB. The somewhat high peak values of the cross-polarization are acceptable for the Arecibo radio telescope since the Gregorian optics stretches the inner ±30° of the feed illumination to almost 90% of the aperture, resulting in very low cross-polarization values over the antenna aperture to the order of −28 dB (see Table 1).

At 8 GHz (Figure 12), there is a decrease in the feed pattern edge taper at 60° due to an oversized OMT circular waveguide diameter. As a result, the antenna aperture illumination (η_{Illum}) decreases, reducing the overall effective aperture efficiency ($\eta_{Aperture}$) of the Arecibo radio telescope, as shown in Table 1.

To analyze the antenna performance with this feed horn, we obtained a spherical wave expansion of the calculated full radiation pattern of the feed horn ($-180° < \theta < +180°$) and used an electromagnetic ray-tracing technique to obtain the fields at the Arecibo

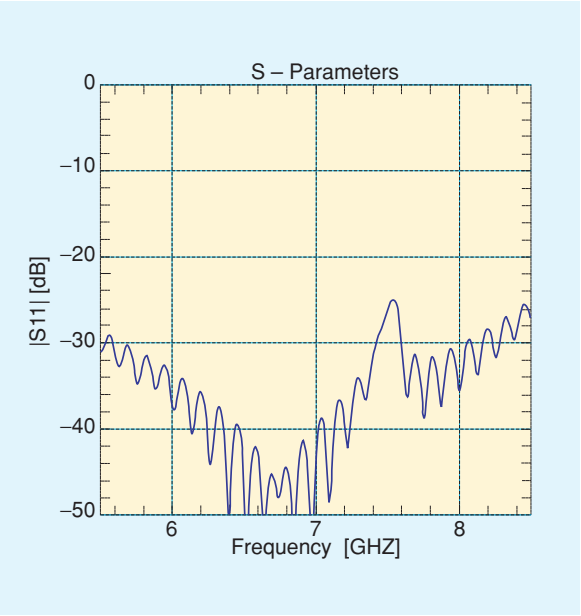

Figure 9. *Calculated horn input reflection coefficient as a function of frequency.*

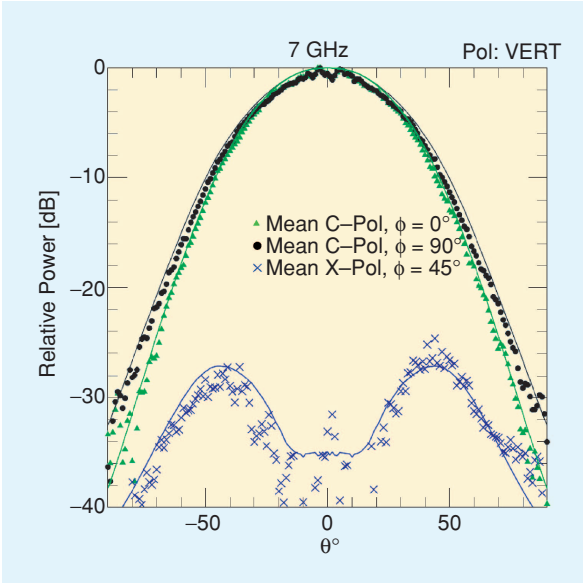

Figure 11. *Calculated (continuous lines) and measured (dots) copolar radiation patters cuts at 0°, 90° and Cross-polar at 45° (Horn–I at 7 GHz).*

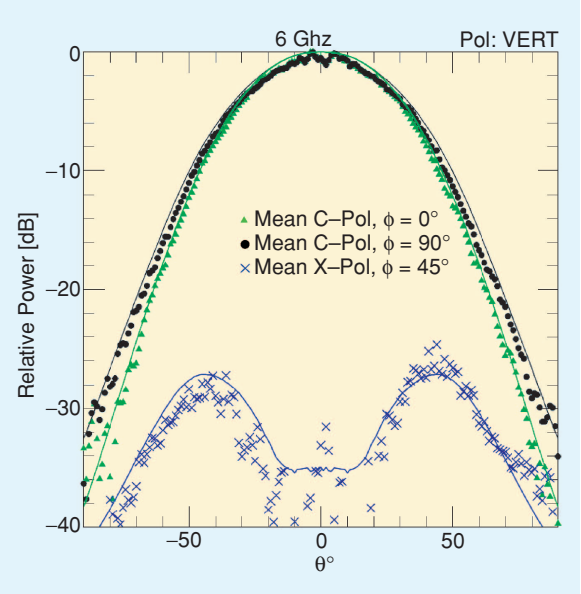

Figure 10. *Calculated (continuous lines) and measured (dots) copolar radiation patters cuts at 0° and 90° and cross polar at 45° (Horn–I at 6 GHz).*

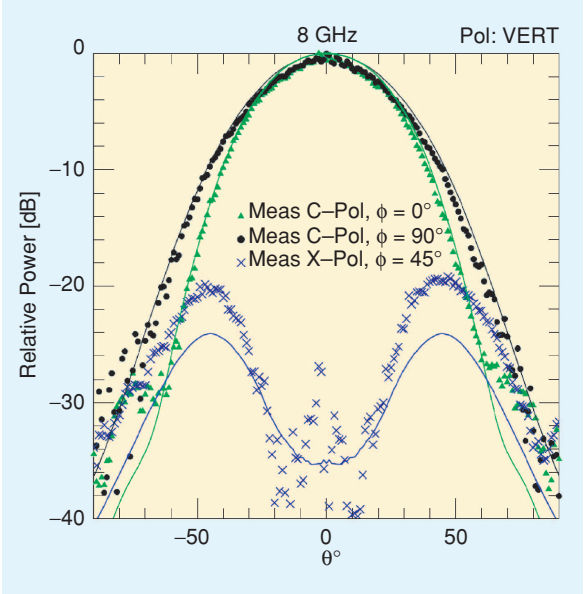

Figure 12. *Calculated (continuous lines) and measured (dots) copolar radiation patters cuts at 0° and 90° and cross-polar at 45° (Horn–I at 8 GHz).*

aperture and in the far field. From these, we calculated the antenna parameters from 6–8 GHz, some of which are presented in Table 1, which includes the aperture efficiency, η_{Aperture} (effective collecting area of the telescope divided by the illuminated area, which is 3.98×10^4 m^2), aperture illumination efficiency, η_{Illum} (reduction in efficiency due to nonuniform illumination of the antenna), 10 dB beam efficiency, η_{Beam} (fraction of total radiated power within −10 dB of peak of power pattern), cross-polarization level in the antenna far field, X-Pol, and the antenna temperature, T_A (includes contributions from the 2.73 K cosmic microwave background radiation, emission from the atmosphere, and radiation from the dome and spillover radiation from the ground). All these values are calculated at the feed horn input flange. Reduction of efficiency due to surface errors is not included.

The calculated values of aperture efficiency include blockage losses, aperture phase efficiencies, and spillover efficiencies not shown individually in the table. Table 1 shows the decrease in aperture efficiency at 8 GHz due to the reduced illumination efficiency.

The calculated cross-polarization values in the antenna far field are below −26 dB. The antenna noise temperature values decrease as a function of frequency due to the reduction of the size of the feed beam.

Thermal Break

The feed horn and the dewar window are kept at room temperature (300 K) while the rest of the signal path starting with the OMT are cooled to 15 K. Hence, there needs to be a device that thermally isolates the 300 K stage from the 15 K stage. This is achieved using a thermal break. A thermal break comprises two waveguides that are separated from each other by a very small gap. A choke groove device is placed at the gap so that the impedance as seen at the wall of the waveguide is close to zero across most of the band. The design of this choke groove is described in the following.

The basic schematic of the choke groove is shown in Figure 13. The parameters to be determined are the location of the coaxial waveguide, R_c, and the height of the groove (or length of the coaxial waveguide), which should be one-quarter of the guide wavelength in the coaxial waveguide, λ_g. This involves a knowledge of the electromagnetic wave propagation both radially outward along the gap and axially along the coaxial waveguide.

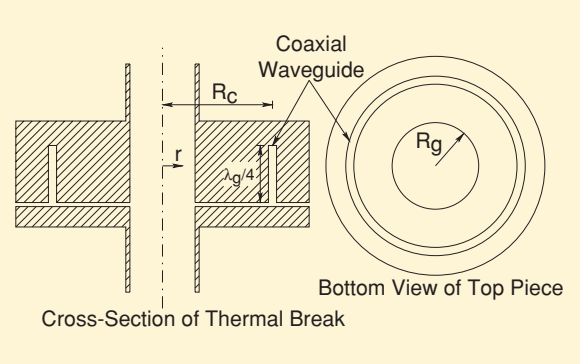

Figure 13. *Schematic of a thermal break with a choke groove. (a) A cross section of the device, which comprises a top piece and a bottom piece that are thermally isolated through stand-offs made from a material like G10 fiberglass. (b) The bottom view of the top piece. The inner radius of the circular waveguide is R_g and that of the choke groove is R_c.*

Figure 14 shows a schematic of the coaxial waveguide, which is treated as a rolled up thin rectangular waveguide. If the height h of the waveguide is small compared to its radius, we can analyze it as if it were not rolled up at all, except for the boundary condition that the field is periodic with period C, where $C = 2\pi R_c$, is the circumference of the waveguide. The direction of the E field will be in the y direction. From Maxwell's equations, the wave propagation equation in the waveguide is

$$\frac{\partial^2 E}{\partial x^2} - \left(k_z^2 - k_0^2\right) E = 0, \tag{1}$$

where $k_0 = 2\pi/\lambda_0$ and λ_0 is the free-space wavelength. Now, the boundary condition requires that the dependence of E on x be of the form $\cos(2\pi nx/C)$. Since the waveguide mode under consideration is TE_{11}, we have $n = 1$. Hence, we have

$$\frac{\partial^2 E}{\partial x^2} + \left(\frac{2\pi}{C}\right)^2 E = 0. \tag{2}$$

From the two equations above, we get

$$k_z = \sqrt{k_0^2 - \left(\frac{2\pi}{C}\right)^2}. \tag{3}$$

The guide wavelength λ_g is given by $2\pi/k_z$, which becomes

$$\lambda_g = \frac{\lambda_0}{\sqrt{1 - \left(\frac{\lambda_0}{2\pi R_c}\right)^2}}. \tag{4}$$

This gives the height of the choke groove, once R_c is determined (as described below).

In the radial waveguide (the section of the gap between the main circular waveguide and the coaxial waveguide), the electric field is a function of only r and θ, where (r, θ) refer to polar coordinates. The field cannot be a function of z as its divergence would then not be zero. From Maxwell's equations, we have

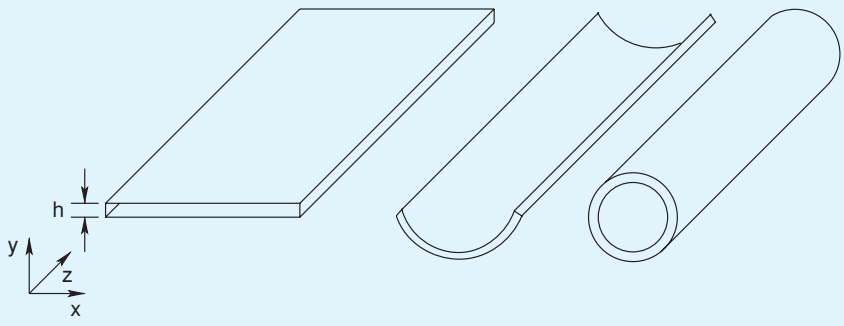

Figure 14. *A coaxial waveguide can be treated as a rolled up thin rectangular waveguide.*

$$\nabla \times \nabla \times E - k_0^2 E = 0. \tag{5}$$

Taking the z component of above gives

$$\begin{aligned}(\nabla \times \nabla \times E)_z =& \frac{1}{r}\frac{\partial}{\partial r}\left(r\frac{\partial E_z}{\partial r}\right) - \frac{1}{r}\frac{\partial}{\partial \theta}\left(\frac{1}{r}\frac{\partial E_z}{\partial \theta}\right) \\ =& k_0^2 E_z. \end{aligned} \tag{6}$$

The angular dependence of E_z must again be proportional to $\cos(n\theta)$, where for the same reason as before, $n = 1$. Thus, the above equation becomes

$$\frac{\partial^2 E_z}{\partial r^2} + \frac{1}{r}\frac{\partial E_z}{\partial r} + \left(k_0^2 - \frac{1}{r^2}E_z\right) = 0. \tag{7}$$

The solutions to this equation are the Bessel functions $J_1(k_0 r)$ and $Y_1(k_0 r)$, and the radial part of E_z is a linear combination of the two:

$$E_z(r) = J_1(k_0 r) + a\, Y_1(k_0 r). \tag{8}$$

The location of the groove (coaxial waveguide) can now be determined as follows. The purpose of the choke groove is to make the gap look like the wall of a normal waveguide, and hence the E field in the gap is zero at $r = R_g$. Hence, the first task is to determine the linear combination of Bessel functions (the parameter a) that will give rise to a zero at $r = R_g$. Then, the location of the groove is given by the value of r that maximizes or minimizes this linear combination. Once R_c is determined, λ_g can be calculated, which gives the height of the groove.

In our case, the circular waveguide had a radius $R_g = 2.48$ cm (0.975 in). Doing the calculation described above, we determined R_c to be 3.51 cm (1.38 in). The guide wavelength in the coaxial waveguide, λ_g, turned out to be 4.42 cm (1.74 in), and hence the groove height was set to 1.10 cm (0.435 in). The gap in the waveguide is set to be as small as practical for better performance and in our case, turned out to be 0.018 cm (0.007 in). We had two thermal breaks in the dewar, one for isolating the 70 K stage from the 300 K stage and another for isolating the 15 K stage from the 70 K stage. This was done so as to reduce the heat load on the second stage of the refrigerator (which nominally cools down to 15 K). Indeed, the use of two thermal breaks lowered the heat load to allow the second stage to cool down to around 10.5 K during actual operation, which in turn lowered ohmic contribution to the receiver noise temperature.

Low-Noise Amplifiers

The low-noise amplifiers used in the receiver utilize a monolithic-microwave integrated circuit (MMIC) that was designed at Caltech [4] and fabricated in the Northrop Grumman semiconductor foundry. The module is shown in Figure 15 with a closeup of the MMIC in Figure 16. The MMIC is the type WBA13, which utilizes three indium-phosphide high-electron-mobility transistors (HEMTs) with 0.1 μm gate length. The amplifiers have extremely low noise (< 4 K) over a very wide bandwidth (4–12 GHz) when cooled to 12 K, as shown in Figure 17. Over 50 of these amplifiers with very repeatable performance have been built at Caltech. At 300 K, the noise temperature of the amplifier is approximately 50 K (0.7 dB noise figure).

Remainder of the Signal Path

The overall signal path in the receiver is shown in Figure 18. The low-noise amplifier is preceded by an isolator and a directional coupler. The isolator was from Passive Microwave Technology and had specifications of 20 dB isolation with an input and output voltage standing wave ratio (VSWR) of 1.24 and an insertion loss of less than 0.38 dB (which was verified through actual measurements). The directional couplers are used for injecting power from a noise diode and are used for calibration purposes during

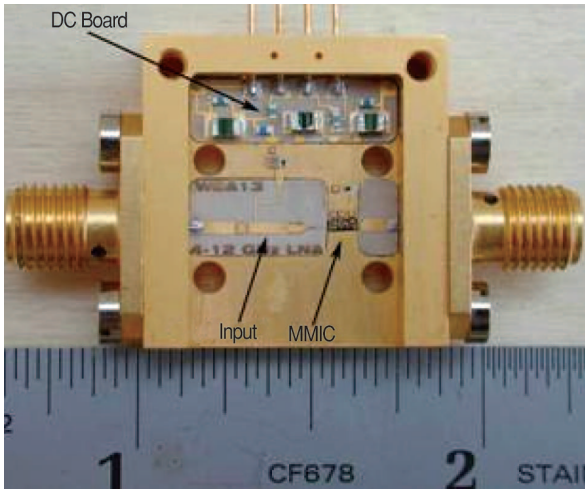

Figure 15. *LNA module with covers removed. The module is comprised of input, output, dc bias circuit boards, and an InP MMIC three-stage amplifier, shown in Figure 16.*

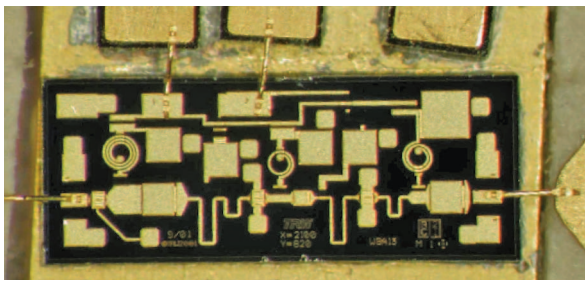

Figure 16. *WBA13 MMIC used in the amplifier. The chip size is 2 mm × 0.73 mm. The bond wires are for input, output, gate, and drain voltage. In addition to the three transistors, the chip contains thin-film resistors and capacitors and spiral inductors. Over 1,000 amplifiers can be produced on one 3-in wafer.*

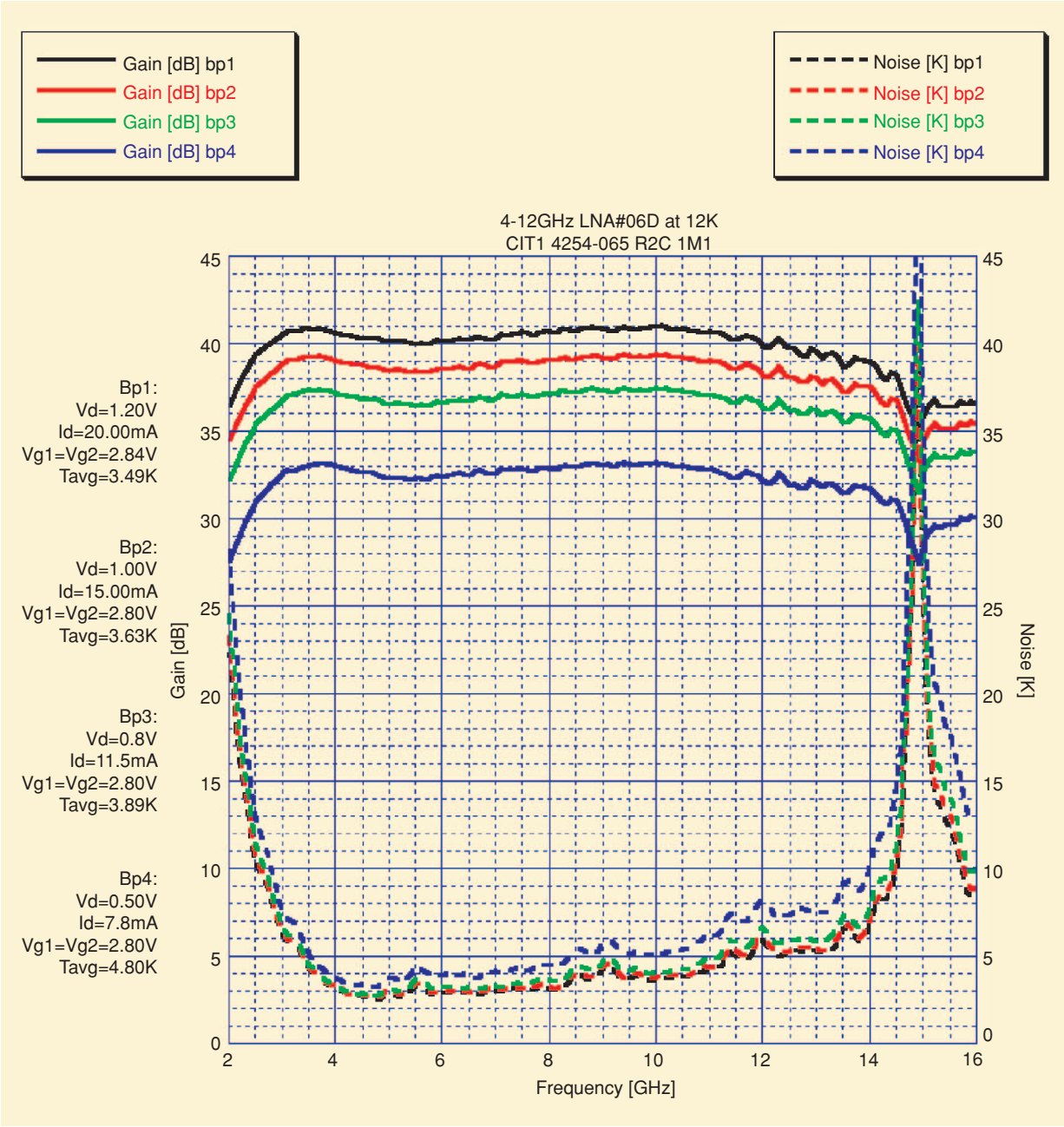

Figure 17. *Measured gain and noise temperature at 12 K at four different bias settings for a typical LNA of the type used in the receiver. The highest bias power of 24 mW results in 41 dB gain and 3.5 K noise averaged from 4–12 GHz, while a lower bias power of 3.9 mW still results in 33 dB gain and 4.8 K average noise.*

astronomical observations. The couplers were from MAC Tech, and had return loss of less than 25 dB, insertion loss of less than 0.15 dB, coupling of 30 ± 1.25 dB, and a directivity better than 30 dB, which were well within specifications.

The output from the low-noise amplifier is then taken out of the dewar and converted to a center frequency of 1.5 GHz. This is in turn transmitted over an optical fiber link to the signal processing area in a building adjacent to the telescope. There, a digital autocorrelation spectrometer produces spectra. Long stainless steel cables with beryllium copper inner conductors were used between the refrigerator stages to minimize conductive heat loads on the refrigerator.

Receiver Noise Temperature

We evaluated the overall noise temperature of the receiver using the Y-factor method. The receiver was mounted such that the feed horn was looking at the sky, which served as the cold load. Then, a piece of Eccosorb absorbing material was placed in front of the horn to serve as the hot load. By measuring the receiver power with the two loads, the noise temperature of the receiver, T_{rx}, can be evaluated by

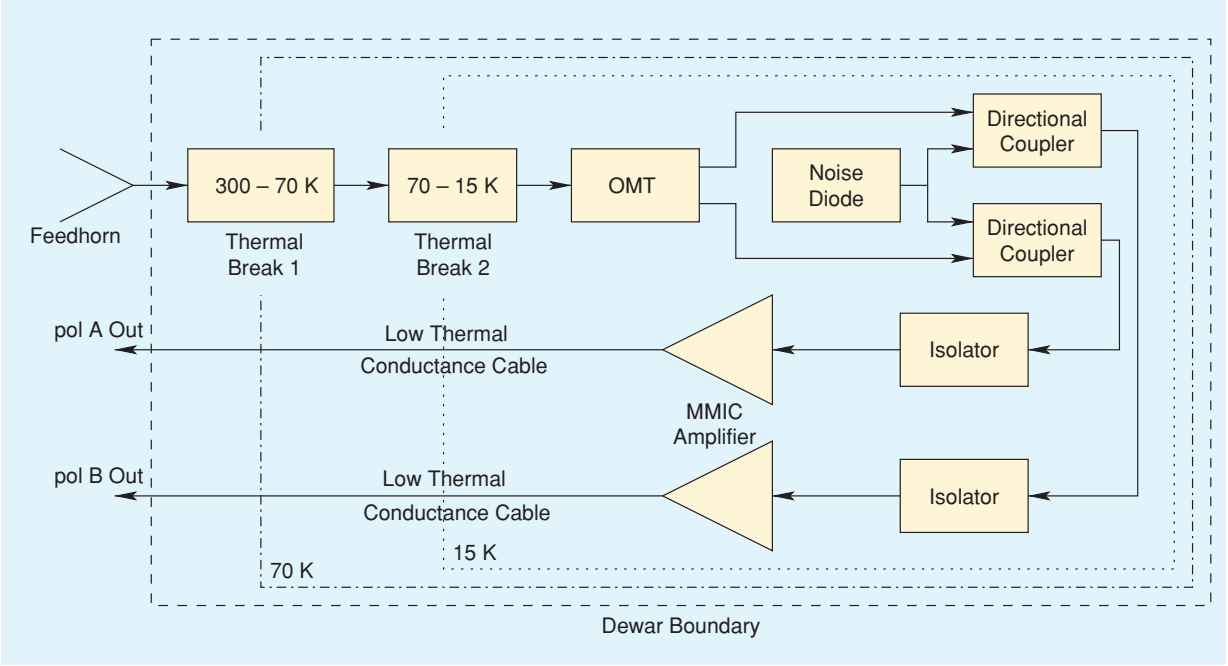

Figure 18. *Schematic of the receiver showing the signal path from the feed horn to the exterior of the dewar.*

$$T_{rx} = \frac{T_{\text{amb}} - YT_{\text{sky}}}{Y - 1}, \tag{9}$$

where T_{amb} is the ambient temperature, T_{sky} is the sky temperature, and $Y = P_{\text{hot}}/P_{\text{cold}}$ is the ratio of the power measured using hot and cold loads.

The sky temperature is the sum of the contribution of the cosmic microwave background and the opacity and emission of the atmosphere, which depend on the amount of precipitable water vapor. The measurements were carried out in the early morning when the sky conditions were clear with relatively low water vapor content (for Arecibo), and we estimated the emission from the sky to be 6.5 K [5]. We made measurements over the course of seven days and averaged the resulting measurements together. The results are shown in Figure 19. Losses from the directional coupler, isolator, and cables contribute to the receiver noise temperature in addition to the low-noise amplifier. Due to the high gain of the low-noise amplifier (~40 dB), the noise contribution from the post-amplifier stage is negligible.

The receiver noise temperature measurement was in turn used to calibrate the noise diodes that would be used for calibration during astronomical observations.

Overall System Performance

The telescope itself makes a significant contribution to the overall system temperature due to spillover and stray radiation. These effects are dependent on the azimuth and zenith angle of the telescope. Thus, the net system temperature ranges from 23–29 K in one polarization (designated pol A in Figures 4 and 5), and 28–34 K in the other polarization (designated pol B), with higher system temperatures occurring at larger zenith angles.

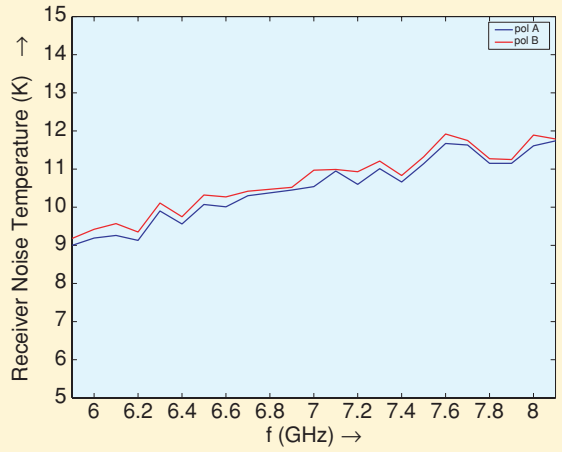

Figure 19. *Measured receiver noise temperature. Note the higher noise temperature for pol B due to the higher insertion loss of the OMT for this polarization.*

The beam response was measured by using a set of raster-scans in azimuth at uniformly and closely spaced zenith-angle offsets about the direction of an astronomical source, B1040 + 123. The scans covering about 36 arcmin^2 were obtained at a suitably fast rate to avoid large changes in the zenith angle in order to minimize the possible uncertainties arising from any associated variations in the telescope performance. The data were recorded at 1 ms intervals with full polarization information and gain was calibrated using a local reference noise source switched at 25 Hz. Four bands of

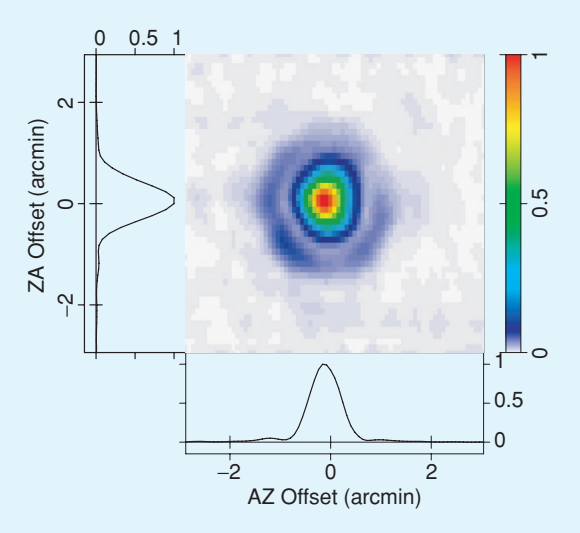

Figure 20. *Normalized beam response mapped as a function of offsets in azimuth and zenith-angle and estimated using full polarization measurements from a set of raster-scans on a continuum source B1040 + 123. The estimates shown here correspond to the response in the Stokes I parameter.*

100 MHz width each around 6.6 GHz were observed with 128 spectral channels per band, and the spectral data were combined later to obtain a band-averaged response. Suitable regridding and interpolation were performed to obtain a beam map with fine and uniform sampling in the azimuth and the zenith-angle offsets. The estimated response in Stokes I is shown in Figure 20. The elliptical beam pattern is a result of the final illumination aperture of diameter 213 × 237 m [6]. The coma side-lobe is apparent around the main response whose angular widths in the two directions are consistent with the expectation. Figure 21 displays two orthogonal cuts sampled through and normalized to the peak response. The coma response is seen to be, on average, below −12 dB of the main beam peak.

At present, the feed horn, isolators, directional couplers, and low-noise amplifiers for the second beam are not installed. Consequently, the receiver is working as a normal single-beam instrument at present. It is expected to be upgraded to a full dual-beam receiver by early 2007.

Conclusions

The combination of the traveling wave OMT device and the ultra-low-noise MMIC amplifiers has allowed us to develop a broadband 6–8 GHz receiver with a noise temperature of around 10 K. The combination of receiver noise and the additional noise contributions by the telescope optics gives an overall receiver temperature of around 28 K and 34 K in the two polarizations. The large collecting area of the telescope gives rise to a system equivalent flux density of around 4.5 Jy at 7 GHz.

References

[1] P.F. Goldsmith, "The second arecibo upgrade," *IEEE Potentials*, vol. 15, pp. 38–43, Aug.–Sept. 1996.

[2] G. Chattopadhyay and J.E. Carlstrom, "Finline ortho-mode transducer for millimeter waves," *IEEE Microwave Guided Wave Lett.*, vol. 9, pp. 339–341, Sept. 1999.

[3] P.J.B. Clarricoats and A.D. Olver, *Corrugated Horns for Microwave Antennas* (IEEE Electromagnetic Waves Series 18). Stevenage, UK: Peregrinus, 1984.

[4] N. Wadefalk and S. Weinreb, "Very low noise amplifiers for very large arrays," in *Proc. Workshop WFF, IEEE IMS2005 Symp.*, Long Beach, CA, June 2005 [CD-Rom].

[5] P.F. Goldsmith, "Calculation of atmospheric emission measured by Gregorian feed horns," NAIC Internal Memo, Sept. 2001.

[6] P.S. Kildal, L.A. Baker, and T. Hagfors, "The arecibo upgrading: Electrical design and expected performance of the dual-reflector feed system," *Proc. IEEE*, vol. 82, pp. 714–724, May 1994.

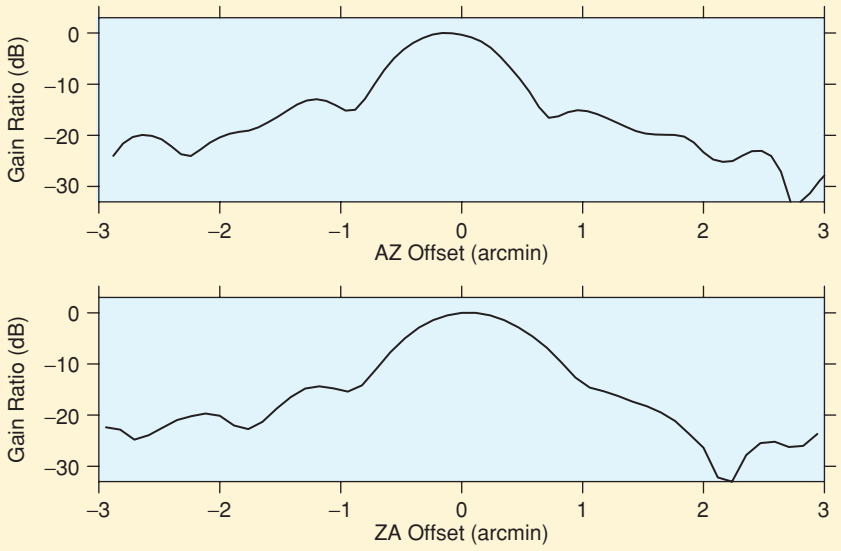

Figure 21. *The beam profiles in azimuth and zenith angle respectively, sampled from the beam-map (shown in Figure 20) as cuts through its peak, are shown in dB scale with respect to the peak response.*